ADVANCED OPTICAL MATERIALS
www.advopticalmat.de

Mixed Microscopic Eu^{2+} Occupancies in the Next-Generation Red LED Phosphor $Sr[Li_2Al_2O_2N_2]:Eu^{2+}$ (SALON:Eu^{2+})

*Freia Ruegenberg, Amador García-Fuente, Markus Seibald, Dominik Baumann, Gregor Hoerder, Tim Fiedler, Werner Urland, Hubert Huppertz, Andries Meijerink, and Markus Suta**

Red-emitting narrow-band phosphors are of utmost importance for next-generation white-light phosphor-converted light-emitting diodes (pc-wLEDs) for improved efficacy and optimized correlated color temperatures. A promising representative crystallizing in an ordered variant of the UCr_4C_4 structure type is $Sr[Li_2Al_2O_2N_2]:Eu^{2+}$ (SALON:Eu^{2+}) emitting at a desirable wavelength of 614 nm. Despite an expected eightfold coordination of the Eu^{2+} ions by four N^{3-} and O^{2-} ions, respectively, the exact local coordination symmetry and a 1:1 ratio between the two types of ligands is not straightforwardly proven by X-ray diffraction. Low-temperature luminescence spectroscopy in conjunction with ligand field theory are powerful alternatives to resolve local features of Eu^{2+} as its excited $4f^65d^1$ configuration reacts sensitively to the polarity of the ligands. The dominant emission at 614 nm shows pronounced vibronic fine structure at 10 K. In addition, weak emission bands can be resolved at 570 and 650 nm even at a low doping concentration of 0.5 mol% and are assigned to Eu^{2+} ions being eightfold coordinated by N^{3-} and O^{2-} ions in a ratio different from 1:1. Due to the feature of *vierer* ring-type channels in SALON:Eu^{2+}, those Eu^{2+} centers are sufficiently close for mutual energy transfer, which is characterized by time-resolved luminescence at 10 K.

1. Introduction

Eu^{2+}-based phosphors have emerged as fruitful candidates for application in next-generation phosphor-converted white light-emitting diodes (pc-wLEDs).[1,2] If Eu^{2+} is embedded in structures with only a few possible metal ion sites, a highly condensed network backbone and high structural rigidity, these phosphors consistently show narrow-band emission.[3,4] This structure–property relationship has been brought close to perfection in the case of $Sr[LiAl_3N_4]:Eu^{2+}$ (SLA:Eu^{2+}), which crystallizes in an ordered variant of the UCr_4C_4 structure type with the space group $P\bar{1}$ (no. 2).[5] This structure type is characterized by so-called *vierer* ring channels that lead to an approximately cubic eightfold coordination of the incorporated cations.[6] Due to the soft covalently binding N^{3-} ions in the coordination environment that exhibit a strong nephelauxetic effect, SLA:Eu^{2+} emits at 650 nm close to the edge of the eye

F. Ruegenberg, H. Huppertz
Institute of General
Inorganic and Theoretical Chemistry
University of Innsbruck
Innrain 80–82, Innsbruck 6020, Austria

A. García-Fuente
Department of Physics
University of Oviedo
Oviedo E-33007, Spain

A. García-Fuente
Nanomaterials and Nanotechnology Research Center CINN
CISC-University of Oviedo
El Entegro E-33424, Spain

The ORCID identification number(s) for the author(s) of this article can be found under https://doi.org/10.1002/adom.202202732.

DOI: 10.1002/adom.202202732

M. Seibald, D. Baumann, G. Hoerder, T. Fiedler
ams-OSRAM International GmbH
Mittelstetter Weg 2 86830, Schwabmünchen, Germany

W. Urland
Private Institute of Theoretical Chemical Physics
Muralto 6600, Switzerland

A. Meijerink, M. Suta
Condensed Matter & Interfaces
Debye Institute for Nanomaterials Sciences
Department of Chemistry
Utrecht University
Princetonplein 1, Utrecht 3584 CC, The Netherlands
E-mail: markus.suta@hhu.de

M. Suta
Inorganic Photoactive Materials
Institute of Inorganic Chemistry
Heinrich Heine University Düsseldorf
Universitätsstraße 1 40225, Düsseldorf, Germany

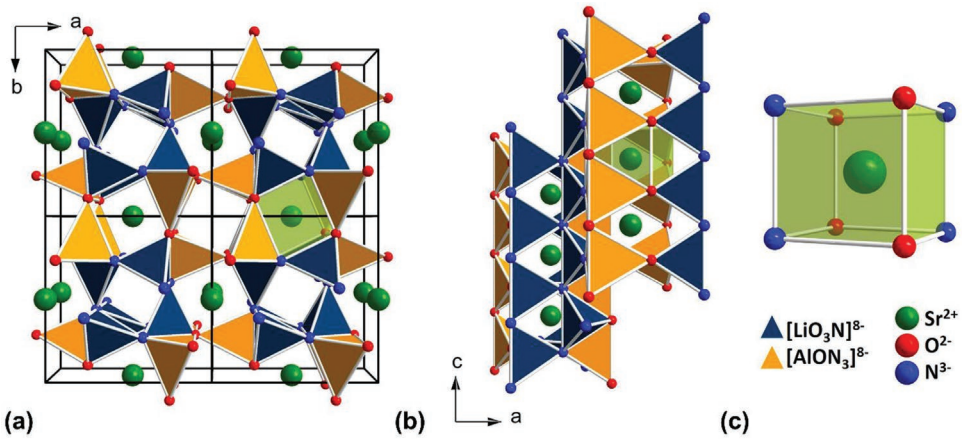

Figure 1. Structure of $Sr[Li_2Al_2O_2N_2]$ (SALON).[8] a) View of the crystal structure along the crystallographic [001] direction showing the relation to the UCr_4C_4 structure type and the vierer rings containing the Sr^{2+} cations. b) Emphasis of the columnar structure along the [001] direction showing the embedding of the Sr^{2+} cation channels in the condensed backbone of $[LiO_3N]^{8-}$ and $[AlON_3]^{8-}$ tetrahedra. c) View on the cube-like coordination sphere of the Sr^{2+} ions with the different types of O^{2-} and N^{3-} ligands resulting in a local $C_{2h}(x)$ symmetry at the Sr sites. Note that the angles in the cube actually slightly deviate from 90° (thus resulting in C_{2h} and not D_{2h} symmetry). The *x* denotes the twofold axis running parallel to the [100] direction.

sensitivity for red light with an effective full width of half maximum (FWHM) of only 1180 cm^{-1} (50 nm).[5] According to standards in the lighting industry, a desirable emission wavelength for a red-emitting phosphor in next-generation pc-wLEDs is between 610 and 620 nm where the eye sensitivity is higher.[7] Using the successful structural feature of SLA:Eu^{2+} together with a different crystal structure and incorporation of slightly harder O^{2-} anions, Hoerder et al. were able to synthesize a phosphor that fulfills the desired criteria with a retained narrow FWHM. This resulted in the phosphor $Sr[Li_2Al_2O_2N_2]:Eu^{2+}$ (SALON:Eu^{2+}, see **Figure 1**) emitting at 614.5 nm with a FWHM of 1286 cm^{-1} (48 nm) at room temperature,[8] representing an illustrative textbook-type example of the exploitation of structure–property relationships and variation in the nature of the chemical bond to generate an applied material with desired properties. Additional exchange with O^{2-} finally results in the UCr_4C_4-type narrow-band emitting phosphor $Sr[Li_3AlO_4]:Eu^{2+}$.[9] Another fully oxide-based class of materials of the UCr_4C_4 structure family are the lithosilicates,[10,11] which were originally prepared by Hoppe's group[12] and have become prominent as potential cyan- and green-emitting phosphors with wide color gamut for display applications.[2,13]

A special feature of SALON:Eu^{2+} is the slightly asymmetric emission band at room temperature. A number of theoretical studies have been published on SALON:Eu^{2+} to explain both the emission wavelength and asymmetry of this emission band.[14,15] A strong argument arises by the vicinity of the Sr^{2+} ions (Sr—Sr distance: 3.184 Å) that lead to an extended vibronic coupling including collective motion of the cations within the channels. A remaining challenge is the unambiguous proof for the location of and compositional ratio between the N^{3-} and O^{2-} ions within the first coordination sphere of Eu^{2+}. Usually, single-crystal X-ray diffraction is the most straightforward structure resolving method for such purposes. However, not only are N and O weak X-ray scatterers based on their low atomic number, but also hard to distinguish because they are neighboring elements in the periodic table. In addition, the presence and exact position of Li^+ cations in this structure are hard to prove by means of X-ray diffraction and is accompanied by strong disorder effects or split positions in case of mobility. In addition, no indications for a super-structure formation are observable in the X-ray diffraction data of SALON:Eu^{2+}, justifying the assignment of O and N positions in the chosen space group in combination with electrostatic calculations.[8] Nevertheless, short-range anion ordering cannot be handled with such average-structure models. Thus, despite its simplicity, X-ray diffraction is pushed to its limitations for such a specific research question. Another method with the capability to resolve the distribution of light elements is electron energy loss spectroscopy (EELS). EELS can potentially discriminate nitrogen from oxygen but is usually only surface-sensitive, requires an advanced high-resolution transmission electron microscopy setup, and the samples need to withstand the incident energies of the electron beam. In fact, SALON:Eu^{2+} decomposes under the conditions of a conventional EELS experiment according to our experience.

High-resolution luminescence spectroscopy can offer a competitive and insightful alternative here. Since the 5d orbitals of Eu^{2+} react sensitively to the local chemical environment and especially to the covalency of the Eu-ligand bonds based on the nephelauxetic effect, it is a suited method to distinguish hard surrounding O^{2-} anions from softer N^{3-} anions despite their isoelectronic character by means of the emission wavelength of the respective $4f^65d^1 \rightarrow 4f^7$ transition of Eu^{2+}. These can be well correlated to advanced ligand-field calculations to gain information about the ratio of different ligands and symmetry in a heteroleptic coordination sphere around Eu^{2+} ions. Resolved vibronic fine structure at cryogenic temperatures ($T < 10$ K) can additionally reveal important structural information if the doping fraction is kept sufficiently low ($x < 0.5$ mol%) to avoid inhomogeneous broadening effects, which has been recently impressively demonstrated in several solid solutions of isostructural alkaline earth fluorides and hydrides, for example.[16] Finally, time-resolved luminescence at various temperatures helps elucidate energy transfer interaction or quenching effects that could also be correlated to the local structure of the Eu^{2+} ions. We have recently shown the power of a combination of single-crystal X-ray diffraction, high-resolution luminescence

spectroscopy and ligand field calculations for resolving delicate structural problems in the case of the UCr_4C_4-type lithooxidosilicate "$K_2Na_2[Li_3SiO_4]_4:Eu^{2+}$", which actually has the composition $K_{1.6}Na_{2.1}Li_{0.3}[Li_3SiO_4]_4:Eu^{2+}$ also containing small Li^+ ions in the cation channels and not only in the tetrahedral network backbone.[17] This motivated us to investigate both the steady-state and time-resolved luminescence of SALON:Eu^{2+} with several doping concentrations (0.1 mol% and 0.5 mol%) at different temperatures and to demonstrate the often still underestimated power that lies in luminescence spectroscopy in conjunction with ligand field calculations to solve structurally advanced problems.

2. Results and Discussion

2.1. High-Resolution Luminescence Spectra of SALON:Eu^{2+} at Low Temperatures

Figure 2a,b depicts the luminescence spectra of SALON: 0.5 mol% Eu^{2+} at 10 K. Note that the regarded Eu2+ concentrations of 0.1% and 0.5% within this work are lower than what is typically used in commercial LED phosphors (>1%) to avoid inhomogeneous broadening that would obscure vibronic fine structure. The photoluminescence excitation spectra are characterized by two broad bands with maxima at 290 and 450 nm, respectively. This demonstrates that SALON:Eu^{2+} can be efficiently excited with a conventional blue-light $In_{1-x}Ga_xN$ LED. SALON:Eu^{2+} crystallizes in an ordered variant of the UCr_4C_4 structure type with the space group $P4_2/m$ (no. 84).[8] The Sr^{2+} or Eu^{2+} ions are located within channels along the [001] direction that are composed by both $[AlON_3]^{8-}$ and $[LiO_3N]^{8-}$ tetrahedra and are coordinated by four N^{3-} and four O^{2-} ions in a cube-like arrangement according to the single-crystal X-ray diffraction data. The cation positions are centrosymmetric according to the space group/site symmetry and give rise to an unusual coordination pattern with four O^{2-} and four N^{3-} ligands in a $C_{2h}(x)$ symmetry (see Figure 1c; x denotes that the C_2 axis lies along the [001] direction within the crystal structure) given the slight deviation of the angles within the cube-like coordination sphere from 90°. However, the very similar Sr/Eu-ligand bond

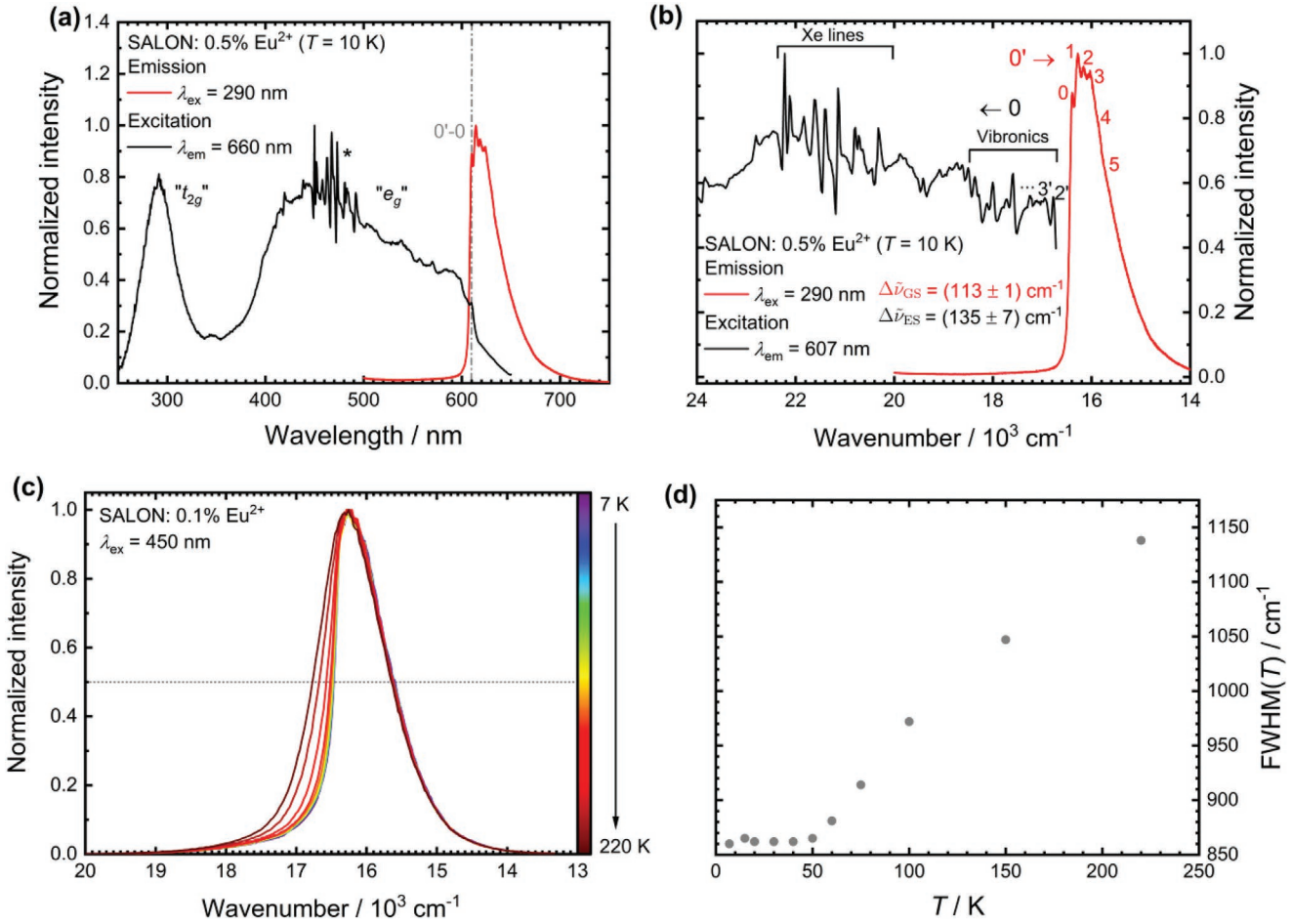

Figure 2. Photoluminescence properties of SALON:Eu^{2+} at cryogenic temperatures (T = 10 K). a) Photoluminescence emission (red, λ_{ex} = 290 nm) and excitation (black, λ_{em} = 660 nm) of SALON:0.5% Eu^{2+} at T = 10 K. The spikes marked with an asterisk stem from Xe lamp lines. The zero-phonon line (ZPL, 0′-0 transition) is indicated. b) Enlarged view to the spectra converted into the wavenumber domain (with Jacobian intensity correction) for the analysis of the vibronic fine structure in the emission (red, λ_{ex} = 290 nm) and excitation (black, λ_{em} = 609 nm) spectra. c) Temperature-dependent emission spectra (λ_{ex} = 450 nm) of SALON:0.1% Eu^{2+} indicating the thermal broadening of the $4f^65d^1 \rightarrow 4f^7$-based emission of Eu^{2+} between T = 7 and 220 K. The spectra have been normalized for better clarity. d) Temperature dependence of the FWHM of the Eu^{2+}-based emission in SALON:Eu^{2+}.

lengths (Sr—N bond length: 2.760(5) Å; Sr—O bond length: 2.659(4) Å) and the diffuse nature of the 5d orbitals could allow the assumption of an apparently experienced cube-like coordination sphere with O_h site symmetry by the Eu^{2+} ions. Under this assumption, the two broad bands of the excitation spectra could be interpreted as the ligand field splitting $10Dq$ between the lower energetic "e_g" and the higher energetic "t_{2g}" ligand field states of the 5d orbitals in a decoupled scheme with an energy difference of around $10Dq_{\text{eff}} \approx 13\ 330\ \text{cm}^{-1}$ [estimated from the energy difference between zero-phonon line (ZPL, at 16 393 cm^{-1}) and onset of the "t_{2g}"-labelled excitation band at 29 720 cm^{-1}]. It is important to stress, however, that this is only an approximation and the real, lower $C_{2h}(x)$ symmetry leads to additional removal of degeneracy of the 5d orbitals. Another characteristic feature is the staircase-like fine structure on the lower energetic excitation band that is usually regarded as a signature of the ^7F_J (J = 0...6) levels of the $4f^6$ core in the excited $4f^65d^1$ configuration. It has, however, been recently demonstrated by Joos et al.[18] (and earlier by Weakliem [19]) by relativistic embedded-cluster CASSCF calculations that this interpretation in a decoupled scheme should be taken with caution and is not strictly applicable but may merely serve as an approximation. In particular, the chemical bonds in the $[EuO_4N_4]^{18-}$ polyhedron have an appreciable covalent character, which should intuitively lead to a stronger interaction between the 4f electrons and the 5d electron. This is in competition to a reduced overlap given the more diffuse nature of the 5d orbitals and the comparably localized character of the 4f orbitals.

Both the low-energy side of the excitation spectrum and high energy side of the emission spectrum of SALON:Eu^{2+} show a pronounced vibronic fine structure and a well-resolved ZPL at 16 393 cm^{-1} (610 nm). It is blue-shifted compared to the reported ZPL of SLA:Eu^{2+} at 15 797 cm^{-1} (633 nm),[5] which is explained by the partial presence of harder O^{2-} ions in the immediate coordination sphere of Eu^{2+}. From the $4f^65d^1 \rightarrow 4f^7$-based emission band at 10 K, a vibronic progression frequency of $\Delta\tilde{\nu}_{\text{GS}} = (113 \pm 1)\ \text{cm}^{-1}$ can be derived, which is high compared to the progression reported in other oxidic host compounds such as SrB_4O_7:Eu^{2+} ($\Delta\tilde{\nu} = 85\ \text{cm}^{-1}$).[20] It is also in very close agreement to the value reported for SLA:Eu^{2+} of around 100 cm^{-1}. This implies strong Eu^{2+}-ligand bonds, as was also recently found in the structurally related oxidosilicates with Eu^{2+} in the smaller cation channels containing Li^+ ions that give rise to a green luminescence with similar vibronic fine structure at 10 K. From the intensity ratio of the $0' \rightarrow 1$ and $0' \rightarrow 0$ vibronic line, it can be derived that the Huang-Rhys-Pekar parameter S must be around 1.4 being very small. Only few examples such as $REPO_4$:Eu^{2+}, Zr^{4+} (RE = Y, Lu) [21] or selected perovskite-derived hydrides and deuterides[22] are known to give rise to $4f^65d^1 \rightarrow 4f^7$-based luminescence with even smaller Huang-Rhys-Pekar factors ($S < 1$). Thus, the Eu-ligand equilibrium bond length in the lowest excited emissive $4f^65d^1$ state and the $4f^7$ ($^8S_{7/2}$) ground level is very similar and barely changes. This is a consequence of the highly condensed network backbone of $[AlON_3]^{8-}$ and $[LiO_3N]^{8-}$ that introduces structural rigidity and does not mechanically allow strong changes in the Eu-ligand distance. In the low energetic part of the excitation spectra of SALON:Eu^{2+}, there is also some vibronic fine structure visible, which allows the derivation of an estimated vibronic progression frequency of $\Delta\tilde{\nu}_{\text{ES}} = (135 \pm 7)\ \text{cm}^{-1}$. The higher value than that derived from the emission spectra is an indication that the chemical bond between Eu^{2+} and the surrounding ligands in the lowest excited $4f^65d^1$ state is slightly stronger than in the $4f^7$ ground state and should give rise to a slightly smaller Eu-ligand equilibrium distance. This has been consistently found in several other $4f^{n-1}5d^1 \rightarrow 4f^n$-emitting lanthanoid ions (including Eu^{2+}) in highly symmetric coordination environments both theoretically and experimentally.[23]

The small effective FWHM of 860 cm^{-1} (37 nm in the wavelength domain) of the emission band at 10 K also agrees very well with the expected value according to the derived Huang-Rhys-Pekar parameter (880 cm^{-1}) from the vibronic fine structure, which can be calculated as:[24]

$$\text{FWHM}\,(0) = 8\sqrt{S \ln 2}\cdot\hbar\omega_{\text{eff}} \tag{1}$$

Both the FWHM and the derived Stokes shift of only around 350 cm^{-1} (derived from the position of the ZPL) at 10 K are expected according to the strong structural rigidity of SALON. It is noteworthy, however, that the $4f^65d^1 \rightarrow 4f^7$ emission band shows an asymmetry. This is partially attributed to the low Huang-Rhys-Pekar parameter that leads to a Pekarian or Poissonian lineshape rather than a Gaussian one at low temperatures. However, we will discuss the full origin of this asymmetry in more detail below. The Huang-Rhys-Pekar parameter for the respective $4f^65d^1 \rightarrow 4f^7$ emission in SLA:Eu^{2+} is slightly larger ($S \approx 2.5$) as estimated from the reported spectra at 10 K.[4] This is reasonable given the softer nature of the N^{3-} ions that allow a slightly higher degree of mechanical flexibility upon excitation/emission than is the case in the SALON partially containing harder O^{2-} ions. At elevated temperatures, the FWHM increases (see Figure 2c,d), which is related to the thermal occupation of the higher vibronic levels in the electronic excited state, from which also Franck–Condon transitions to the electronic ground state can occur. For that purpose, the dilute 0.1 mol%-doped sample was regarded to minimize inhomogeneous broadening effects. Another potential source for the thermal broadening may be a thermal population of higher energetic $4f^65d^1$ electronic levels.

2.2. Potential Anion Disorder within Powdered SALON Samples

Upon variation of the excitation wavelength to a wavelength region where the absorption by the main Eu^{2+} site is low, additional emission bands are observed at both lower and higher energies than the dominant red emission with maximum at 614 nm (see **Figure 3**). The corresponding excitation spectra are similarly broad and imply the presence of Eu^{2+} with a different coordination pattern than the one with four O^{2-} and four N^{3-} ligands arranged in $C_{2h}(x)$-symmetric fashion. Since the structure of SALON only allows incorporation of Eu^{2+} in eightfold coordinated sites arranged in a cubic-like geometry, these results must be interpreted as sites with different N:O ratios. The two identified additional emission bands have roughly the same integral and it can be assumed at this low doping concentration of only 0.5 mol% that the respective Eu^{2+} centers must have mutually similar concentrations. While the emission bands at higher energies should contain an excess in the harder O^{2-}

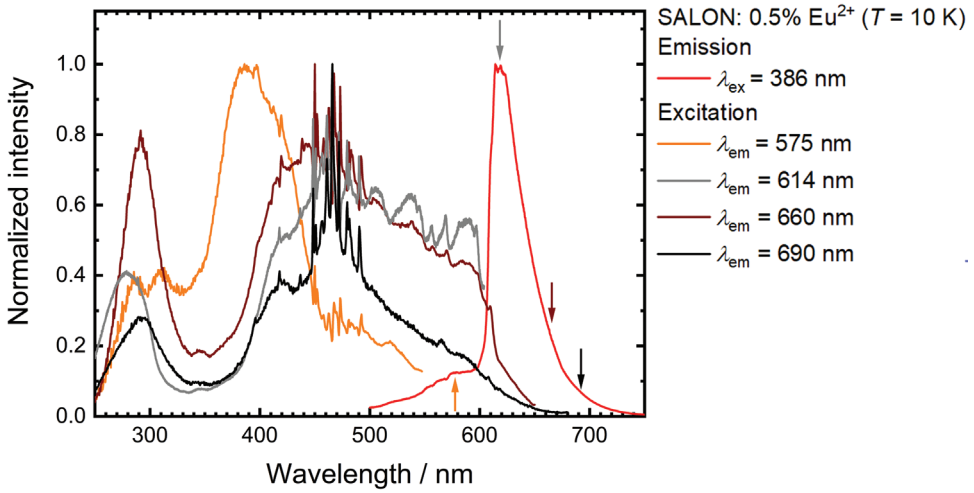

Figure 3. Detection of additional emission bands in SALON:0.5% Eu^{2+} by selective excitation with λ_{ex} = 386 nm (red) at T = 10 K. The respective excitation spectra upon detection of the different emission bands (λ_{em} = 575 nm, orange; λ_{em} = 614 nm, grey; λ_{em} = 660 nm, brown; λ_{em} = 690 nm, black) are also depicted.

ions, those at lower energies should be related to sites, in which Eu^{2+} is coordinated by more N^{3-} than O^{2-} ions. Accordingly, there appears to be a microscopically present change in the N:O ratio in the coordination spheres around the Eu^{2+} ions within powdered samples of SALON. While ordered SLA:Eu^{2+} leads to an ZPL emission at 633 nm and a maximum of 653 nm at 10 K, a respective emission in the fully oxygen ordered congener $Sr[Li_3AlO_4]:Eu^{2+}$ is expected in yellow or orange range. It was shown that lithooxidoaluminates with compositions close to the indicated one also crystallize in a UCr_4C_4-type structure with a tetragonal crystal system (space groups $P4/n$ [no. 85] or $I4/m$ [no. 87]).[25] Based on the positions of the emission bands in SALON:Eu^{2+} (614 nm) and SLA:Eu^{2+} (653 nm) at room temperature, it is possible to estimate that the expected peaking position in anion-ordered $Sr[Li_3AlO_4]:Eu^{2+}$ lies at around 575 nm, in good agreement with experimental findings (λ_{em} = 570 nm, FWHM = 1540 cm^{-1}, or 46 nm in the wavelength domain).[9] In this context, it is also important to mention that Hoerder et al. have prepared a series of SALON-related Eu^{2+}-doped phosphors with both cation and anion disorder in the condensed network built up by the tetrahedra and the composition $SrAl_{2+z}Li_{2-z}O_{2(1+z)}N_{2(1-z)}$, in which the $4f^65d^1 \rightarrow 4f^7$-based emission of Eu^{2+} can be tuned from the orange (z = 0.66) to the deep red (z = 0.12) range.[26] As expected, however, the anion disorder leads to an inhomogeneous broadening of the Eu^{2+}-related emission bands at room temperature and a much lower effective quenching temperature of around $T_{1/2}$ = 450 K. In contrast, both SLA:Eu^{2+} and SALON:Eu^{2+} are characterized by quenching temperatures well above 600 K,[5,8] This demonstrates the relevance of anion ordering in these structures for the efficiency of these phosphors for pc-wLEDs. Since thermal quenching at such low temperatures has not been observed for our investigated powdered sample of SALON:Eu^{2+}, we expect a strong anion ordering of the compound.

A possible structural interpretation for the observation of the additional emission bands is the following. Upon incorporation of higher doping fractions of Eu^{2+} into SALON, substitution of the occupied Sr sites is expected. In powdered SALON:Eu^{2+}, the actual microscopic anion composition within these occupied channels may vary and there could also be local cube-like environments with different O:N ratios than 1:1. This is a microscopic effect and not readily expected for a single crystal of SALON:Eu^{2+} with a clearly defined and fully ordered anion composition of the occupied channel. However, even in a crystalline powder, a major part of the Sr sites is fully anion-ordered with a well-defined O:N ratio given the observable vibronic fine structure and the known high thermal quenching temperatures. This is also suggested by Rietveld refinement of the X-ray powder diffraction patterns (see Figure S1, Supporting Information). It is noteworthy that the structure of SALON also incorporates channels that contain vierer rings coordinated by solely N^{3-} or O^{2-}, respectively, but without any occupied cation sites.[8] Occupation of these originally empty cation sites with Eu^{2+} could also explain the observation of additional emission bands at around 600 (pure O^{2-}-based coordination) and 650 nm (pure N^{3-}-based coordination, similar to SLA:Eu^{2+} [5]). However, single-crystal structure refinement found no evidence for the presence of Eu^{2+} in these channels in any of the luminescent UCr_4C_4-type compounds being studied in detail so far. Moreover, considering the cube-like polyhedra that Eu^{2+} would occupy in this case, it becomes clear that the additional emission bands do not match with previous experience on the relationship between emission properties and volumes of the coordination polyhedra.[27]

The solely N-coordinated unoccupied site in one of the empty channels in the SALON structure has an estimated volume of only 24.3 $Å^3$ (see Figure S2, Supporting Information), which would expectedly give rise to a strongly red-shifted luminescence upon occupation by Eu^{2+} ions. As a demonstrative example, the size of the coordination polyhedron in SLA:Eu^{2+} is 36.9 $Å^3$ at red luminescence with an emission maximum at 650 nm.[5] It is important to note that the calculated polyhedral volumes do not necessarily represent the eventual conditions in the real structure. It can be assumed that the presence of an activator ion leads to a slight distortion of the polyhedra, but nevertheless a significant red shift of the Eu^{2+}-based emission

into the near infrared would be expected when incorporated into this otherwise unoccupied nitride channel in SALON. The situation is similar for the potential Eu^{2+} position with exclusive O coordination in the otherwise unoccupied channel: here, the polyhedron in eightfold coordination would have a volume of 30.7 Å^3. Known UCr_4C_4 oxide phosphors such as the alkali lithosilicate $K_{1.6}Na_{2.1}Li_{0.3}[Li_3SiO_4]_4$:$Eu^{2+}$ emit in the cyan wavelength range with comparable polyhedral volumes containing Eu^{2+}.[17] Consequently, it can be assumed that the additional emission bands at 575 and 660 nm are not due to an incorporation of Eu^{2+} within the unoccupied channels of the SALON structure but likely arise from Eu^{2+} substituting the cube-like Sr sites.

In order to assess whether Eu^{2+} substituting Sr sites within a coordination polyhedron with deviating O:N ratio could account for the additional emission bands and also to give an idea about the quality of the analyzed samples, Rietveld refinement was performed. For this purpose, single-crystal data of SALON were first used as a starting model for the refinement of the main phase. As a secondary phase, a theoretical disordered $Sr[Li_2Al_2O_2N_2]$ was simulated based on the crystal structure of $Sr[Mg_2Al_2N_4]$, a UCr_4C_4-type compound crystallizing in the space group $I4/m$ (no. 87) with cation/anion disorder (mixed site occupation).[3] Replacing the Mg position by Li and splitting the N position into O and N with a site occupation factor of 0.5 each, the simulated phase has the same mean composition as SALON but without any ordering effects. This average structure model enables the possibility of local O:N variation around the Sr position at first approximation in the real structure while maintaining the mean composition of the material. The Rietveld refinement resulted in 4.49(4) wt% phase fraction of SALON simulated in $I4/m$ (no. 87), which supports the hypothesis that locally varied anionic environments around the activator ion site in the Sr polyhedron could cause the additional emission bands as the Rietveld fit can be significantly improved by adding such a secondary phase. Nevertheless, a small inhomogeneity in the powder sample would cause the same effect on the refinement as the O:N ratio in the final phosphor is mainly affected by the mixing process of the starting materials which cannot be fully controlled on an atomic level.

2.3. Ligand-Field Calculations for Different Anion Compositions in the $[EuO_{8-x}N_x]^{(14+x)-}$ Polyhedra

We performed density functional theory (DFT) and ligand field simulations of SALON:Eu^{2+} to independently assess the effect of possible different O:N ratios in the cube-like coordination environment of Eu^{2+} ions on the emission wavelength of the $4f^65d^1 \rightarrow 4f^7$ transition. For that purpose, we simulated a SALON supercell with Eu^{2+} occupying a Sr site both in the ground ($[Xe]4f^7$) and excited ($[Xe]4f^65d^1$) configuration. The distance between the Eu^{2+} ion and the ligands are $d_{Eu\text{-}O}$ = 2.614 Å, $d_{Eu\text{-}N}$ = 2.743 Å in the $4f^7$-based ground and $d_{Eu\text{-}O}$ = 2.601 Å, $d_{Eu\text{-}N}$ = 2.712 Å) in the lowest excited $4f^65d^1$-related state. The average equilibrium Eu-ligand bond lengths are slightly shorter in the lowest excited state, which agrees with earlier theoretical and experimental findings.[22]

To reproduce the luminescence properties of Eu^{2+}, we need to go beyond mean-field methods that do otherwise not allow to obtain the complete Eu^{2+} manifolds.[18] Instead, we use our DFT results to generate a multielectronic Hamiltonian in the basis of the different $4f^7$ and $4f^65d$ configurations that includes the effect of electron–electron interaction, spin-orbit coupling and the ligand field.[28] In **Figure 4**a, we show the simulated excitation spectra, where we find a gap between "e_g" and "t_{2g}" similar

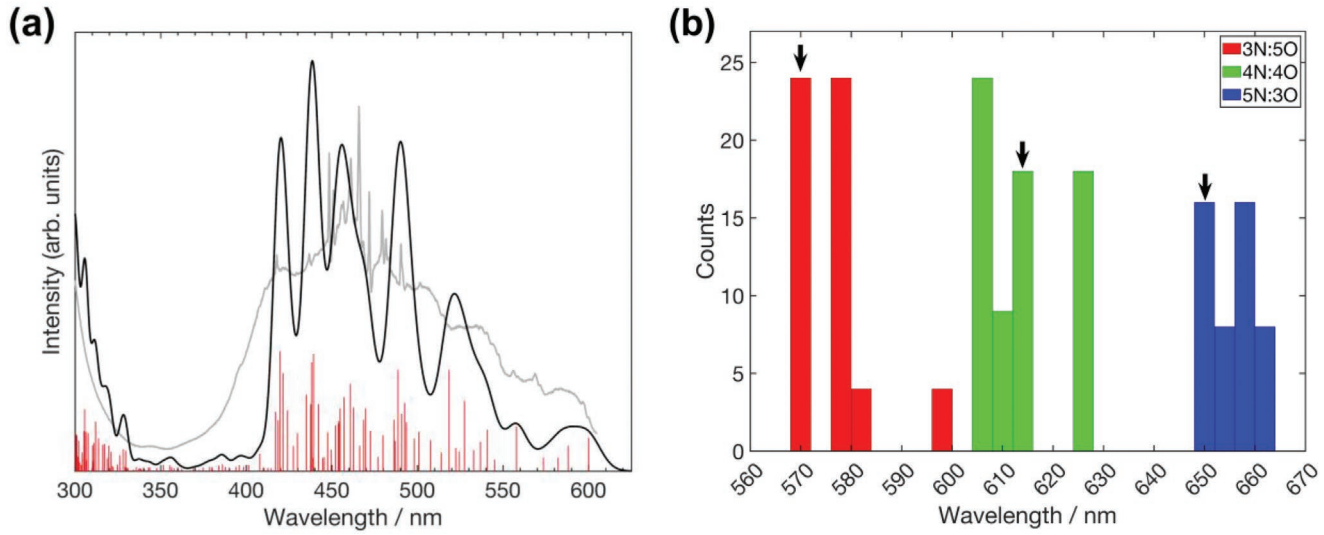

Figure 4. a) Simulated excitation spectra of SALON:Eu^{2+} (black curve) with red vertical lines showing the wavelengths of the different transitions between multielectronic states. Their height is proportional to the transition probability. The underlying grey spectrum is an experimental excitation spectrum of SALON:0.1% Eu^{2+} at T = 10 K (λ_{em} = 615 nm). b) Different emission wavelengths obtained for different cube-like distributions of O^{2-} and N^{3-} ions around Eu^{2+} with ratios 3N:5O ($[EuO_5N_3]^{17-}$), 4N:4O ($[EuO_4N_4]^{18-}$), and 5N:3O ($[EuO_3N_5]^{19-}$). The counts on the ordinate denote the number of symmetry-equivalent possibilities to place the O^{2-} and N^{3-} ligands in a given ratio on the corners of the slightly distorted cube. Arrows show the emission wavelengths obtained for the expected 4N:4O distribution and for the 3N:5O and 5N:3O distributions obtained by simple O ↔ N exchange from the $C_{2h}(x)$-symmetric coordination entity according to the structural refinement.

to that shown in the experimental data. In fact, the ligand field levels extracted from DFT show $10Dq \approx 13\ 000\ cm^{-1}$, which is in very good agreement with the estimated value ($13\ 330\ cm^{-1}$) from the experimental spectra at 10 K (see Figure 2).

As the real symmetry around Eu^{2+} in SALON is actually $C_{2h}(x)$ (see Figure 1c), the 5d orbitals lose their degeneracy completely. This allows us to rewrite the ligand field matrix of the system in terms of the angular overlap model (AOM).[29] We obtain $e_\sigma(O) = 9024\ cm^{-1}$, $e_\sigma(N) = 8058\ cm^{-1}$, $e_\pi(O) = 3826\ cm^{-1}$, and $e_\pi(N) = 1925\ cm^{-1}$. As expected, it generally is $e_\sigma > e_\pi$ indicating that the σ-type orbital overlaps between the 5d orbitals of Eu^{2+} and the 2p ligand orbitals of O^{2-} and N^{3-} is stronger than the π-type overlap. Additionally, the smaller values for the N^{3-} ligands are a consequence of the larger size of this anion and the related longer Eu-ligand bond, which also leads to a decrease in the orbital overlap and thus, the AO parameters.

Based on the structural input of the Eu-ligand distances and arrangement within a $[EuO_{8-x}N_x]^{(14+x)-}$ ($x = 0...8$) unit, we can reassemble the ligand field matrix by varying desirable coordination patterns with different O:N ratios around the Eu^{2+} ion.

The different emission wavelengths are obtained by exact diagonalization of our multielectronic Hamiltonian with the new ligand field matrix and defined by the energy difference between the lowest excited $4f^65d^1$ state and the $4f^7$ ground state in the excited state equilibrium geometry. The results are depicted in Figure 4b. We have also varied the different possible relative arrangements of the O^{2-} and N^{3-} ligands for a given fixed ratio of the two anions within the cube-like environment of Eu^{2+}. Out of the $2^8 = 256$ possibilities to set up a cube-like environment around the Eu^{2+} ions with two types of ligands (O^{2-} and N^{3-}), for example, $\binom{8}{4} = 70$ include a configuration with four O^{2-} and four N^{3-} ligands, out of which only selected configurations are symmetry-equivalent (see Figure 4b). It is found that arrangements of O^{2-} and N^{3-} in a 1:1 ratio ($[EuO_4N_4]^{18-}$), but with other symmetries than the elucidated $C_{2h}(x)$ symmetry with alternating O^{2-}/N^{3-} ligands according to X-ray diffraction only slightly affect the emission wavelength (see different green bars in Figure 4b). This is, however, not sufficient to explain the additionally observed peaks in the experimental emission spectra. On the other hand, variation of the O:N ratio to 5:3 ($[EuO_5N_3]^{17-}$) or 3:5 ($[EuO_3N_5]^{19-}$) leads to calculated emission wavelengths in the range of 570 (excess O^{2-}) and 650 nm (excess N^{3-}) dependent on the type of symmetry of the respective arrangement. The emission wavelengths resulting from arrangements of the ligands with slight O or N excess show a much closer agreement to the experimentally observed emission wavelengths of the additional low-intensity bands (see Figure 4a). It should be noted that the current parametrization only includes the anionic ligand contributions to the overall ligand field potential, while the proximity of the repulsive Sr^{2+} cations with only 3.184 Å may also have a non-negligible impact on the calculated overall emission energy encoded in a negative e_σ contribution. An impact of the surrounding Sr^{2+} cations within the channel of SALON was also anticipated by Bouquiaux et al.,[14] and similar features were already reported for advanced AOM of $CsMgBr_3:Eu^{2+}$ [30] and also indicated in the AOM of the absorption spectra of lazulite-type oxidephosphates such as β-$Fe_2O(PO_4)$ or $FeTi_2O_2(PO_4)_2$.[31]

2.4. Time-Resolved Luminescence and Energy Transfer between Eu^{2+} Sites of Different Anion Composition in SALON

Besides steady-state spectra, time-resolved luminescence studies are an important diagnostic tool to confirm or even identify the nature of radiative transitions and elucidate potential interaction processes. **Figure 5** depicts the representative luminescence decay curves of SALON:0.1% Eu^{2+} and SALON:0.5% Eu^{2+} acquired upon excitation at $\lambda_{ex} = 441$ nm and detection of the emission at $\lambda_{em} = 614$ nm at 10 K. The luminescence decay is single exponential for both doping fractions of 0.1% and 0.5% Eu^{2+} (see Figure 5a). In SALON:0.1% Eu^{2+}, a radiative decay time of $\tau = (0.83 \pm 0.03)$ µs is observed at 10 K, which is in very good agreement with what is expected for a $4f^65d^1 \leftrightarrow 4f^7$ transition of Eu^{2+} in inorganic hosts. Even for a doping concentration as low as $x = 0.5$ mol%, a slight decrease in the luminescence decay time to $\tau = (0.75 \pm 0.02)$ µs is observed. The slight decrease of the luminescence decay time with increasing doping concentration is an indication for energy transfer between different Eu^{2+} ions. Given the structural feature of large columnar cation channels with mutual cation distances of only 3.184 Å within one channel, energy transfer between different Eu^{2+} ions is structurally strongly favored.

At room temperature, the luminescence decay times in both SALON:0.1% Eu^{2+} and SALON:0.5% Eu^{2+} are slightly higher than at 10 K. This is representatively shown for the 0.1%-doped sample in Figure 5b. Such an observation is a well-known feature of Eu^{2+}-related luminescence and explained by the fact that the lowest excited states in the $4f^65d^1$ configuration have dominant spin octet character based on Hund's rules. Thus, the $4f^65d^1 \rightarrow 4f^7(^8S_{7/2})$ transition has a slightly more spin-allowed character at low temperatures. At elevated temperatures, there is an increasing population of excited $4f^65d^1$ states with stronger spin sextet ($S = 5/2$) character, which leads to a slightly elongated luminescence decay time at room temperature (SALON:0.1% Eu^{2+}: $\tau = (0.86 \pm 0.01)$ µs; SALON:0.5% Eu^{2+}: (0.79 ± 0.02) µs).[11,32]

It should be noted, however, that spin is already only intermediately well-defined for the excited $4f^65d^1$ states of Eu^{2+} since spin-orbit coupling is non-negligible anymore for this ion.

Unlike the dominant red emission, the small blue-shifted and red-shifted emission bands assigned to Eu^{2+} ions with slightly different N:O ratios in their coordination sphere in SALON:0.5% Eu^{2+} show luminescence decay curves with clear signatures of an energy transfer (see Figure 5c). Upon detection of the emission at 575–600 nm, the luminescent decay is multiexponential with components of $\tau_1 = (0.07 \pm 0.01)$ µs, $\tau_2 = (0.55 \pm 0.01)$ µs ($\lambda_{em} = 575$ nm) and $\tau_1 = (0.10 \pm 0.01)$ µs, $\tau_2 = (0.54 \pm 0.02)$ µs ($\lambda_{em} = 600$ nm).

The presence of an initial fast average decay and a slower decay component are typical signatures of a donor ion in an energy transfer process. The long component of this decay is still slightly shorter than the (radiative) decay time of the main emission at 614 nm. This is attributed to a photonic effect as the radiative decay time usually increases with increasing emission wavelength due to the lower photon density of states at longer wavelengths ($\tau_{rad} \propto \lambda_{em}^3$),[33] which is even generally quantitatively fulfilled for the different emitting Eu^{2+} centers in SALON:0.5% Eu^{2+} (see Figure S3, Supporting Information). It

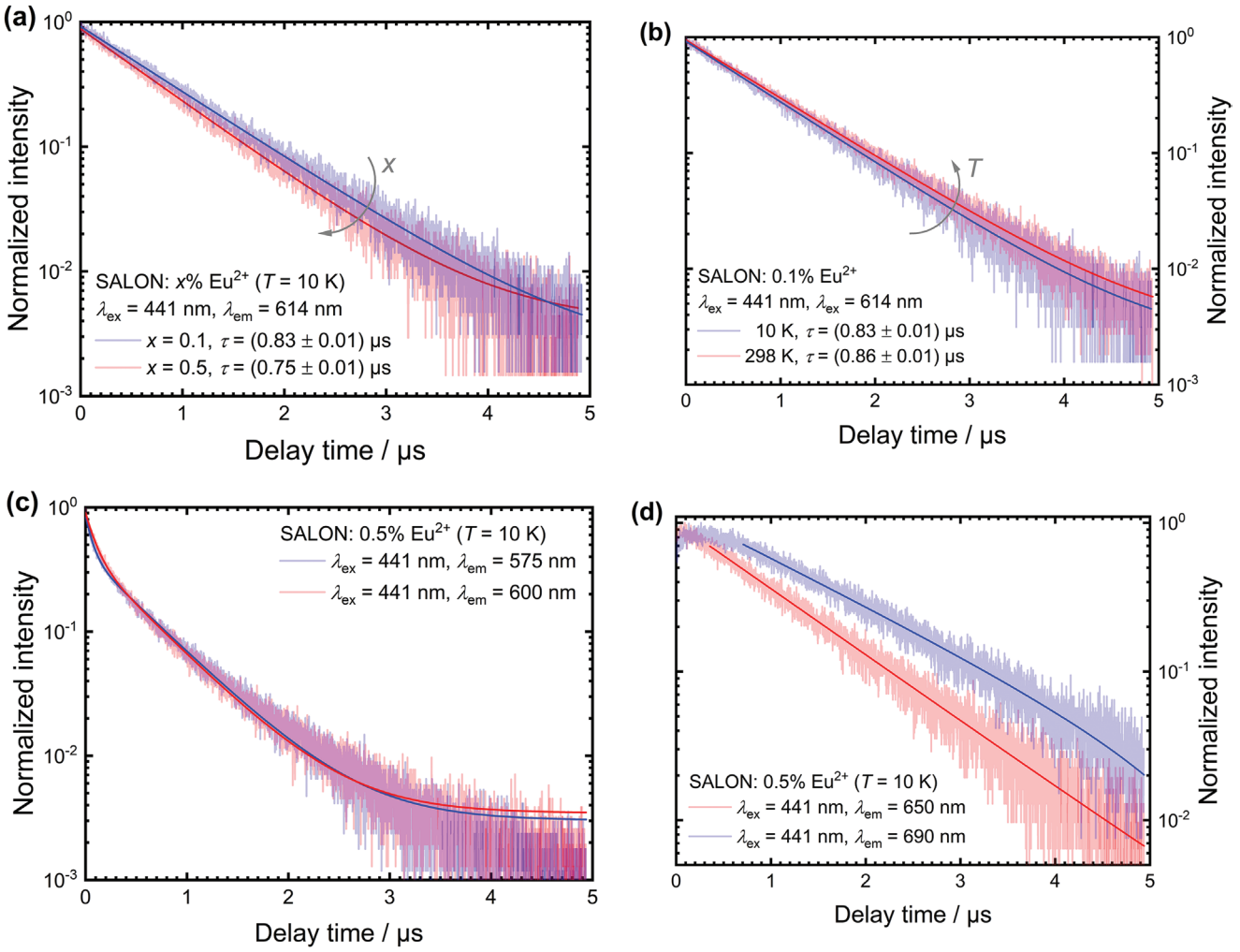

Figure 5. Time-resolved photoluminescence studies on SALON:Eu^{2+} upon excitation with a pulsed laser source at λ_{ex} = 441 nm. a) Luminescence decay curves of the main emission at λ_{em} = 614 nm in SALON:*x*% Eu^{2+} with $x = 0.1$ (cyan) and $x = 0.5$ (blue) at $T = 10$ K indicating the shortening upon increase in doping fraction. Solid lines correspond to single exponential fits (including constant background terms). b) Luminescence decay curves of the main emission at λ_{em} = 614 nm in SALON:0.1% Eu^{2+} at $T = 10$ K (blue) and $T = 298$ K (red) illustrating the increase in decay time upon increasing temperature. Solid lines correspond to single exponential fits (including constant background terms). c) Luminescence decay curves of the orange emission at λ_{em} = 575 and 600 nm in SALON:0.5% Eu^{2+} at $T = 10$ K. Solid lines correspond to biexponential fits. d) Luminescence decay curves of the deep red emission at λ_{em} = 650 and 690 nm in SALON:0.5% Eu^{2+} at $T = 10$ K. Solid lines correspond to single exponential fits of the decay component. See **Table 1** for values of the decay times.

should be noted, however, that there are also other contributions to the luminescence decay time. Variations in the refractive index $n(\lambda)$ also affect the luminescence decay time. However, in the red range of the visible spectrum, the dispersion of the refractive index is usually very weak only. In addition, there is a contribution from the electric dipole transition matrix element $|\mu_{ED}|^2 \propto |\langle 4f|r|5d\rangle|^2$ to the luminescence decay time according to the Golden rule by Dirac and Fermi. A more covalent Eu-ligand bond is related to a spatially more extended 5d wave function, which generally reduces the overlap between 4f and 5d orbitals. However, as has been shown in an extensive study on different Eu^{2+}-activated (complex) oxides, the general variation in this transition dipole matrix element is surprisingly minor (usually less than 20%) even if the emission wavelength varies over the whole visible range.[34] The general correlation of the observed luminescence decay times in SALON:Eu^{2+} with λ_{em}^3 (see Figure S3, Supporting Information) also confirm that the contribution from the emission wavelength appears to be the dominant one in this host compound.

Table 1. Extracted decay components from the time-resolved studies on SALON:*x*% Eu^{2+} (x = 0.1, 0.5) of the main emission at λ_{em} = 614 nm (excitation at λ_{ex} = 441 nm).

Temperature/doping fraction *x*%	$x = 0.1$	$x = 0.5$
10 K	$\tau = (0.83 \pm 0.01)$ µs	$\tau = (0.75 \pm 0.01)$ µs
298 K	$\tau = (0.86 \pm 0.01)$ µs	$\tau = (0.79 \pm 0.02)$ µs

In the longer wavelength domain at 650–690 nm, the time-resolved luminescence shows an initial rise component followed by an exponential decay (see Figure 5d). Such a behavior is typical for an acceptor in an energy transfer process. It is

helpful to quantitatively assess this. As the rise components were too short within the regarded time range to allow reasonable fits, we regarded the well-detectable maxima of the luminescence decay curves. The expected maximum after an initial rise is given by:

$$t_{\max,\mathrm{est}} = \frac{\ln\left(\frac{\tau_2}{\tau_1}\right)}{\tau_1^{-1} - \tau_2^{-1}} \quad (2)$$

where $\tau_1 < \tau_2$. If we insert the found components from the multiexponential decay at 575–600 nm into Equation (2), we find $t_{\max,\mathrm{est}} = 0.16$ µs and $t_{\max,\mathrm{est}} = 0.20$ µs using the decay components for $\lambda_{\mathrm{em}} = 575$ nm and $\lambda_{\mathrm{em}} = 600$ nm, respectively. These values are close to the experimentally observed maximum in the time-resolved luminescence of the centers emitting at 650–690 nm ($t_{\max,\mathrm{exp}} = 0.12$ µs for $\lambda_{\mathrm{em}} = 650$ nm and $t_{\max,\mathrm{exp}} = 0.21$ µs for $\lambda_{\mathrm{em}} = 690$ nm). This confirms that the weak emission bands at 575–600 and 650–690 nm belong to Eu^{2+} donor and acceptor ions mutually interacting in an energy transfer process, respectively. The decay component of the acceptor ions is longer ($\tau = (0.98 \pm 0.01)$ µs ($\lambda_{\mathrm{em}} = 650$ nm) and (1.37 ± 0.02) µs ($\lambda_{\mathrm{em}} = 690$ nm)) than the luminescence decay time of the Eu^{2+} ions emitting at 614 nm (see **Table 2**), which is again attributed to a photonic effect. Thus, the Eu^{2+} ions at sites with different N:O ratios in SALON cannot be microscopically far apart and interact via an energy transfer. The nearest-neighbor distance between two cation sites within different occupied cation channels is 5.628 Å according to the single-crystal structural data. If we now consider two Eu^{2+} ions within one cation channel with a mutual distance of only 3.184 Å, a simple shortening of the luminescence decay time based on an intra-channel interaction is reasonable. In contrast, the efficiency of a hypothetical energy transfer between Eu^{2+} ions in the otherwise empty fully O^{2-}-coordinated and the fully N^{3-}-coordinated sites, respectively, is already lowered by a factor of $(5.628/3.184)^6 \approx 30$ solely based on a distance dependence argument. The observation of a rise component in the time-resolved signal of the emission band beyond 650 nm despite an otherwise efficient electric dipole–electric dipole-type energy transfer can be related to the low doping fraction of only 0.5 mol% that reduces the probability for close contact or clustering of Eu^{2+} ions with coordination environments with different O:N ratios in the occupied vierer ring channel. On the other hand, the mutual nearest-neighbor cation distance within this channel in the structure of SALON:Eu^{2+} is very small. In agreement to that, the time-resolved signal of the main emission at 614 nm due to Eu^{2+} ions in an eightfold coordination by both O^{2-} and N^{3-} in a 1:1 ratio already shortens upon a concentration increase from 0.1% to only 0.5%. In summary, we assign the asymmetry of the Eu^{2+}-based emission in powdered SALON not only to the Pekarian lineshape arising from the structural rigidity. Another aspect is the presence of other emitting Eu^{2+} ions in an eightfold coordination with different O:N ratios. These results demonstrate the power that a combination of steady-state and time-resolved luminescence studies in conjunction with advanced ligand field calculations have together with advanced single-crystal and powder diffraction methods to elucidate local structural effects with cost-effective and simple methods.

Table 2. Extracted decay components from the time-resolved studies on SALON:0.5 mol% Eu^{2+} of the other emission bands at 10 K (excitation at $\lambda_{\mathrm{ex}} = 441$ nm).

Emission wavelength λ_{em}/nm	τ_1/µs	τ_2/µs
575	0.07 ± 0.02	0.55 ± 0.01
600	0.10 ± 0.01	0.54 ± 0.02
650	–*	0.98 ± 0.01
690	–*	1.37 ± 0.02

*not accurately measurable

3. Conclusions

We have investigated the luminescence properties of $Sr[Li_2Al_2O_2N_2]:Eu^{2+}$ (SALON:Eu^{2+}) with low doping fractions ($x \leq 0.5$ mol%) at 10 K and demonstrated that high-resolution luminescence spectroscopy can serve as a complementary structural tool in cases, in which X-ray diffraction comes to its limitations. It was shown that SALON:Eu^{2+} shows a similarly well-resolved vibronic fine structure as SLA:Eu^{2+} with a zero-phonon line at 16 390 cm^{-1} (610 nm) and a Huang-Rhys-Pekar parameter of $S = 1.4$. This low value and the consequently low emission FWHM of 860 cm^{-1} (31 nm) and Stokes shift of 350 cm^{-1} at 10 K can be related to the highly condensed network of $[AlON_3]^{8-}$ and $[LiO_3N]^{8-}$ tetrahedra and the related structural rigidity. Upon variation of the excitation wavelength, additional low-intensity emission bands were observed in SALON:Eu^{2+} at elevated doping concentrations both at lower (575–600 nm) and higher wavelengths (650–690 nm) than the dominant emission band with maximum at 614 nm. This result indicates that microscopically, the Eu^{2+} ions cannot be solely coordinated by four O^{2-} and four N^{3-} ions in a $C_{2h}(x)$-symmetric fashion, but that there must be also eightfold coordinated sites with different N:O ratios present in powdered microcrystalline SALON. Both Rietveld refinement on powdered samples and ligand field simulations also suggest such a possibility. In contrast, the structural solution based on single-crystal X-ray diffraction suggests a fully anion-ordered structure, which is generally in line with the observation of a well-resolved vibronic fine structure at 10 K, small FWHM (860 cm^{-1}) and Stokes shift (350 cm^{-1}). According to time-resolved luminescence studies at 10 K, these centers also mutually interact via energy transfer processes, which mean that they cannot be far apart within the structure of SALON. Overall, the luminescence properties of Eu^{2+} within this compound can be closely correlated to the local surrounding structure of this emissive ion and are a complementary tool to X-ray diffraction, which comes to its limitations in the local structure elucidation of this compound.

4. Experimental Section

Synthesis: A powder sample of $Sr[Li_2Al_2O_2N_2]:Eu^{2+}$ was obtained by a solid-state reaction similar to reference.[8] The starting materials Al_2O_3 (15.69 g, 153.8 mmol, Sinochem Hebei type C), Li_3N (5.37 g, 154 mmol, Materion), EuF_3 (0.238 g, 1,14 mmol, Materion), and a pre-synthesized aluminate precursor (28.75 g, synthesized using Sr_3N_2 [Materion] and

AlN [Tokuyama]) were mixed and placed inside of a Ni crucible. They were then heated in a tube furnace to 700 °C in a stream of forming gas (7.5% H_2 in N_2) and held at that temperature for 3 h. The resulting product was ground, refilled into the Ni crucible, and heated for a second time. After heating to 775 °C in a stream of forming gas (7.5% H_2 in N_2) and holding this temperature for another 3 h the final product was obtained as a fine red powder. Washing in ethanol yielded a sample of high purity.

Powder X-Ray Diffraction: Powder data were collected on a STOE STADI P diffractometer (Mo-$K_{\alpha 1}$ radiation, λ = 0.7093 Å) with a Ge(111) monochromator and in transmission mode with a Mythen 1K detector (PSD). Rietveld refinement was performed using the software TOPAS 4.2 to evaluate the presence of a secondary phase.

Steady-State and Time-Resolved Photoluminescence Spectroscopy: All photoluminescence excitation and emission spectra were acquired on a FLS920 Edinburgh Instruments spectrometer, equipped with a 450 W Xe lamp as the excitation source, a double Czerny-Turner excitation grating monochromator (0.22 m) blazed at 300 nm and a single Czerny-Turner emission monochromator (0.11 m) blazed at 500 nm. An R928 Hamamatsu photomultiplier tube was used as a detector. All spectra were corrected for lamp intensity, detector response, and grating efficiency. For cryogenic (T = 10 K) and temperature-dependent measurements below room temperature, the samples were cooled in an Oxford Instruments Liquid Flow He cryostat with an external temperature control unit. Luminescence decay measurements were also recorded on the same setup using a pulsed diode laser (441 nm, temporal pulse width ≈75 ps, Edinburgh Instruments) with adjustable repetition rate as the excitation source and an H74220-60 photomultiplier as the detector. The time-resolved signal was detected using a time-correlated single-photon counting card (Edinburgh Instruments) connected to the photomultiplier.

Simulations: DFT simulations were performed with the Vienna ab initio simulation package (VASP) [35] exploiting the projector-augmented wave (PAW) method[36] to reproduce the interaction between the valence and the core electrons.[37] The Perdew–Burke–Ernzerhof (PBE) approximation was used for the exchange–correlation potential.[38] Structural relaxation of supercells containing 288 atoms with periodic boundary conditions was performed. Atomic positions were allowed to relax until all Hellmann–Feynman forces where smaller than 5×10^{-5} eV Å^{-1}. The results of eigenenergies and eigenstates obtained from Vienna ab initio simulation package (VASP) were used to parametrize a multielectronic Hamiltonian that includes electron–electron, spin-orbit, and ligand field interactions finally parametrized in the angular overlap framework.[28]

Supporting Information

Supporting Information is available from the Wiley Online Library or from the author.

Acknowledgements

M.S. is grateful for a material cost allowance from the Fonds der Chemischen Industrie e.V. and funding from the "Junges Kolleg" of the North-Rhine Westphalian Academy of Sciences and Arts. A.G.-F. acknowledges funding of the project PGC2018-094783 (MCIU/AEI/FEDER, EU) and Asturias FICYT under grant AYUD/2021/51185 with the support of FEDER funds. Parts of this work are funded by the German Federal Ministry of Economic Affairs and Climate Action (Bundesministerium für Wirtschaft und Klimaschutz) in the frame of the Important Project of Common European Interest (IPCEI) on microelectronics.

Open access funding enabled and organized by Projekt DEAL.

Conflict of Interest

The authors declare no conflict of interest.

Data Availability Statement

The data that support the findings of this study are available from the corresponding author upon reasonable request.

Keywords

Eu^{2+}, light-emitting diodes, narrow-band red emitter, $Sr[Li_2Al_2O_2N_2]$ (SALON), UCr_4C_4-type phosphors

Received: November 16, 2022
Revised: January 13, 2023
Published online: February 25, 2023

[1] a) J. L. Leaño, M.-H. Fang, R.-S. Liu, *ECS J. Solid State Sci. Technol.* **2018**, *7*, R3111; b) P. Pust, P. J. Schmidt, W. Schnick, *Nat. Mater.* **2015**, *14*, 454; c) C. C. Lin, A. Meijerink, R.-S. Liu, *J. Phys. Chem. Lett.* **2016**, *7*, 495; d) A. Meijerink, *Sci. China Mater.* **2019**, *62*, 146; e) R. Mueller-Mach, G. Mueller, M. R. Krames, H. A. Höppe, F. Stadler, W. Schnick, T. Jüstel, P. Schmidt, *Phys. Status Solidi A* **2005**, *202*, 1727; f) H. A. Höppe, *Angew. Chem., Int. Ed.* **2009**, *48*, 3572; g) M. Zeuner, S. Pagano, W. Schnick, *Angew. Chem.* **2011**, *123*, 7898; h) M. Zeuner, S. Pagano, W. Schnick, *Angew. Chem., Int. Ed.* **2011**, *50*, 7754; i) R.-J. Xie, N. Hirosaki, *Sci. Technol. Adv. Mater.* **2007**, *8*, 588; j) R.-J. Xie, N. Hirosaki, Y. Li, T. Takeda, *Materials* **2010**, *3*, 3777; k) X. Luo, R.-J. Xie, *J. Rare Earths* **2020**, *38*, 464; l) X. Qin, X. Liu, W. Huang, M. Bettinelli, X. Liu, *Chem. Rev.* **2017**, *117*, 4488.

[2] a) Y. Q. Li, A. C. A. Delsing, G. de With, H. T. Hintzen, *Chem. Mater.* **2005**, *17*, 3242; b) Y. Q. Li, K. V. Ramanujachary, S. E. Lofland, G. de With, H. T. Hintzen, *J. Mater. Res.* **2006**, *21*, 396; c) R.-J. Xie, H. T. Hintzen, *J. Am. Ceram. Soc.* **2013**, *96*, 665; d) M. Zhao, Q. Zhang, Z. Xia, *Acc. Mater. Res.* **2020**, *1*, 137.

[3] P. Pust, F. Hintze, C. Hecht, V. Weiler, A. Locher, D. Zitnanska, S. Harm, D. Wiechert, P. J. Schmidt, W. Schnick, *Chem. Mater.* **2014**, *26*, 6113.

[4] a) S. Schmiechen, H. Schneider, P. Wagatha, C. Hecht, P. J. Schmidt, W. Schnick, *Chem. Mater.* **2014**, *26*, 2712; b) S. Schmiechen, P. Strobel, C. Hecht, T. Reith, M. Siegert, P. J. Schmidt, P. Huppertz, D. Wiechert, W. Schnick, *Chem. Mater.* **2015**, *27*, 1780.

[5] P. Pust, V. Weiler, C. Hecht, A. Tücks, A. S. Wochnik, A.-K. Henß, D. Wiechert, C. Scheu, P. J. Schmidt, W. Schnick, *Nat. Mater.* **2014**, *13*, 891.

[6] R. K. Behrens, W. Jeitschko, *Monatsh. Chem.* **1987**, *118*, 43.

[7] US Department of Energy, "Solid state lighting research and development plan",https://www.energy.gov/sites/prod/files/2016/06/f32/ssl_rd-plan_%20jun2016_2.pdf, **2016** (accessed: November 2022).

[8] G. J. Hoerder, M. Seibald, D. Baumann, T. Schröder, S. Peschke, P. C. Schmid, T. Tyborski, P. Pust, I. Stoll, M. Bergler, C. Patzig, S. Reißaus, M. Krause, L. Berthold, T. Höche, D. Johrendt, H. Huppertz, *Nat. Commun.* **2019**, *10*, 1824.

[9] D. Bichler, S. Dallmeir, G. Plundrich, M. Vorsthove, S. Peschke, J. Strube-Knyrim, J. Thoma, C. Koch, P. C. Schmid, C. Stoll, WO2020245282A1, **2020**.

[10] a) D. Dutzler, M. Seibald, D. Baumann, H. Huppertz, *Angew. Chem.* **2018**, *130*, 13865; b) D. Dutzler, M. Seibald, D. Baumann, H. Huppertz, *Angew. Chem., Int. Ed.* **2018**, *57*, 13676; c) D. Dutzler, M. Seibald, D. Baumann, F. Philipp, S. Peschke, H. Huppertz, *Z. Naturforsch. B* **2019**, *74*, 535; d) H. Liao, M. Zhao, M. S. Molokeev, Q. Liu, Z. Xia, *Angew. Chem., Int. Ed.* **2018**, *57*, 11728; e) H. Liao, M. Zhao, M. S. Molokeev, Q. Liu, Z. Xia, *Angew. Chem.* **2018**, *130*, 11902; f) H. Liao, M. Zhao, Y. Zhou, M. S. Molokeev, Q. Liu,

Q. Zhang, Z. Xia, *Adv. Funct. Mater.* **2019**, *29*, 1901988; g) M. Zhao, H. Liao, L. Ning, Q. Zhang, Q. Liu, Z. Xia, *Adv. Mater.* **2018**, *30*, 1802489; h) M. Zhao, Y. Zhou, M. S. Molokeev, Q. Zhang, Q. Liu, Z. Xia, *Adv. Opt. Mater.* **2019**, *7*, 1801631.

[11] M.-H. Fang, C. O. M. Mariano, K.-C. Chen, J.-C. Lin, Z. Bao, S. Mahlik, T. Lesniewski, K.-M. Lu, Y.-R. Lu, Y.-J. Wu, H.-S. Sheu, J.-F. Lee, S.-F. Hu, R.-S. Liu, J. P. Attfield, *Chem. Mater.* **2021**, *33*, 1893.

[12] a) R. Werthmann, R. Hoppe, *Z. Anorg. Allg. Chem.* **1984**, *509*, 7; b) B. Nowitzki, R. Hoppe, *Rev. Chim. Miner.* **1986**, *23*, 217; c) R. Hofmann, B. Nowitzki, R. Hoppe, *Z. Naturforsch. B* **1985**, *40*, 1441; d) K. Bernet, R. Hoppe, *Z. Anorg. Allg. Chem.* **1991**, *592*, 93; e) J. Hofmann, R. Brandes, R. Hoppe, *Z. Anorg. Allg. Chem.* **1994**, *620*, 1495.

[13] M. Zhao, H. Liao, M. S. Molokeev, Y. Zhou, Q. Zhang, Q. Liu, Z. Xia, *Light: Sci. Appl.* **2019**, *8*, 38.

[14] J. Bouquiaux, S. Poncé, Y. Jia, A. Miglio, M. Mikami, X. Gonze, *Adv. Opt. Mater.* **2021**, *9*, 2100649.

[15] a) R. Shafei, D. Maganas, P. J. Strobel, P. J. Schmidt, W. Schnick, F. Neese, *J. Am. Chem. Soc.* **2022**, *144*, 8038; b) M. R. Amin, P. Strobel, W. Schnick, P. J. Schmidt, A. Moewes, *J. Mater. Chem. C* **2022**, *10*, 9740.

[16] A. Mutschke, T. Wylezich, A. D. Sontakke, A. Meijerink, M. Hoelzel, N. Kunkel, *Adv. Opt. Mater.* **2021**, *9*, 2002052.

[17] F. Ruegenberg, A. García-Fuente, M. Seibald, D. Baumann, S. Peschke, W. Urland, A. Meijerink, H. Huppertz, M. Suta, *Adv. Opt. Mater.* **2021**, *9*, 2101643.

[18] J. J. Joos, P. F. Smet, L. Seijo, Z. Barandiarán, *Inorg. Chem. Front.* **2020**, *7*, 871.

[19] H. A. Weakliem, *Phys. Rev. B* **1972**, *6*, 2743.

[20] A. Meijerink, J. Nuyten, G. Blasse, *J. Lumin.* **1989**, *44*, 19.

[21] a) J. Zeler, A. Meijerink, D. Kulesza, E. Zych, *J. Lumin.* **2019**, *207*, 435; b) J. Zeler, M. Sulollari, A. Meijerink, M. Bettinelli, E. Zych, *J. Alloys Compd.* **2020**, *844*, 156096.

[22] N. Kunkel, A. Meijerink, H. Kohlmann, *Phys. Chem. Chem. Phys.* **2014**, *16*, 4807.

[23] a) J. L. Pascual, Z. Barandiarán, L. Seijo, *Phys. Rev. B* **2007**, *76*, 104109; b) Z. Barandiarán, L. Seijo, *J. Chem. Phys.* **2003**, *119*, 3785; c) Z. Barandiarán, N. M. Edelstein, B. Ordejón, F. Ruipérez, L. Seijo, *J. Solid State Chem.* **2005**, *178*, 464; d) P. A. Tanner, C. S. K. Mak, N. M. Edelstein, K. M. Murdoch, G. Liu, J. Huang, L. Seijo, Z. Barandiarán, *J. Am. Chem. Soc.* **2003**, *125*, 13225; e) S. Mahlik, B. Kukliński, Y. M. Yen, R. S. Meltzer, M. Grinberg, *J. Lumin.* **2008**, *128*, 715; f) S. Mahlik, K. Wiśniewski, M. Grinberg, R. S. Meltzer, *J. Phys.: Condens. Matter* **2009**, *21*, 245601; g) S. Mahlik, M. Grinberg, L. Shi, H. J. Seo, *J. Phys.: Condens. Matter* **2009**, *21*, 235603; h) M. de Jong, D. Biner, K. W. Krämer, Z. Barandiarán, L. Seijo, A. Meijerink, *J. Phys. Chem. Lett.* **2016**, *7*, 2730; i) R. Valiente, F. Rodríguez, J. González, H. U. Güdel, R. Martín-Rodríguez, L. Nataf, M. N. Sanz-Ortiz, K. Krämer, *Chem. Phys. Lett.* **2009**, *481*, 149; j) H. Ramanantoanina, W. Urland, A. García-Fuente, F. Cimpoesu, C. Daul, *Chem. Phys. Lett.* **2013**, *588*, 260.

[24] B. Henderson, G. F. Imbusch, *Optical Spectroscopy of Inorganic Solids*, Oxford University Press, Oxford, New York **1989**.

[25] A. Ooishi, Y. Michiue, S. Funahashi, T. Takeda, N. Hirosaki, *Acta Crystallogr., Sect. B: Struct. Sci., Cryst. Eng. Mater.* **2020**, *76*, 76.

[26] G. J. Hoerder, S. Peschke, K. Wurst, M. Seibald, D. Baumann, I. Stoll, H. Huppertz, *Inorg. Chem.* **2019**, *58*, 12146.

[27] M.-H. Fang, C. O. M. Mariano, P.-Y. Chen, S.-F. Hu, R.-S. Liu, *Chem. Mater.* **2020**, *32*, 1748.

[28] A. García-Fuente, F. Baur, F. Cimpoesu, A. Vega, T. Jüstel, W. Urland, *Chem. - Eur. J.* **2018**, *24*, 16276.

[29] a) C. E. Schäffer, C. K. Jørgensen, *Mol. Phys.* **1965**, *9*, 401; b) C. K. Jørgensen, R. Pappalardo, H.-H. Schmidtke, *J. Chem. Phys.* **1963**, *39*, 1422; c) W. Urland, *Chem. Phys.* **1976**, *14*, 393; d) M. Suta, F. Cimpoesu, W. Urland, *Coord. Chem. Rev.* **2021**, *441*, 213981; e) M. Buchhorn, R. J. Deeth, V. Krewald, *Chem. - Eur. J.* **2022**, *28*, e202103775.

[30] H. Ramanantoanina, F. Cimpoesu, C. Göttel, M. Sahnoun, B. Herden, M. Suta, C. Wickleder, W. Urland, C. Daul, *Inorg. Chem.* **2015**, *54*, 8319.

[31] M. Schöneborn, R. Glaum, *Z. Anorg. Allg. Chem.* **2007**, *633*, 2568.

[32] a) C. K. Duan, A. Meijerink, R. J. Reeves, M. F. Reid, *J. Alloys Compd.* **2006**, *408–412*, 784; b) J. P. Spoonhower, M. S. Burberry, *J. Lumin.* **1989**, *43*, 221; c) P. Kisliuk, H. H. Tippins, C. A. Moore, S. A. Pollack, *Phys. Rev.* **1968**, *171*, 336; d) T. Tsuboi, P. Silfsten, *J. Phys.: Condens. Matter* **1991**, *3*, 9163.

[33] D. Toptygin, *J. Fluoresc.* **2003**, *13*, 201.

[34] S. H. M. Poort, A. Meijerink, G. Blasse, *J. Phys. Chem. Solids* **1997**, *58*, 1451.

[35] a) G. Kresse, J. Hafner, *Phys. Rev. B* **1993**, *47*, 558; b) G. Kresse, J. Furthmüller, *Phys. Rev. B* **1996**, *54*, 11169.

[36] P. E. Blöchl, *Phys. Rev. B* **1994**, *50*, 17953.

[37] G. Kresse, D. Joubert, *Phys. Rev. B* **1999**, *59*, 1758.

[38] J. P. Perdew, K. Burke, M. Ernzerhof, *Phys. Rev. Lett.* **1996**, *77*, 3865.